J. Earth Syst. Sci. (2024)133 57
https://doi.org/10.1007/s12040-023-02253-4

Mapping of old coal mine galleries near railway track using electrical resistivity tomography and magnetic approaches in Tundu, Jogidih Colliery, Jharia Coalfield, India

Saurabh Srivastava[1], Rajwardhan Kumar[1], Sanjit Kumar Pal[1,*] and R M Bhattacharjee[2]

[1] *Department of Applied Geophysics, Indian Institute of Technology (Indian School of Mines) Dhanbad, Dhanbad 826 004, India.*
[2] *Department of Mining Engineering, Indian Institute of Technology (Indian School of Mines) Dhanbad, Dhanbad 826 004, India.*
**Corresponding author. e-mail: sanjitism@gmail.com*

MS received 15 June 2023; revised 30 October 2023; accepted 31 October 2023

Underground galleries possess random subsidence threats if they are not treated well. Threats even become multifold when these galleries are located somewhere in the vicinity of the railway tracks. So, checking the stable ground formation or the health of the subsurface formation near railway tracks and mapping the galleries are very important tasks for the sake of the environment, economy and lives. Galleries under the present study are associated with the coal seam-X and seam-XA of the Jogidih Colliery of Jharia Coalfield. Seven electrical resistivity tomography (ERT) profiles and magnetic surveys were performed at a side of the railway track to characterize the subsurface formation near railway tracks and to detect the gallery and its extension. Both ERT and magnetic data analysis suggest the presence of some galleries at a certain distance from the railway tracks. Moreover, combined analysis of ERT and magnetic data suggests that ground within ∼20 m from the railway tracks is found to be stable with homogeneous compact formation.

Keywords. Electrical resistivity tomography; magnetic; void detection; old mine gallery mapping.

1. Introduction

Mapping the galleries and checking their ground conditions near the railway tracks are always challenging. It is highly prioritized in the coal mining sector since it is related to the safety and security of the environment and lives. It adds an immense sense of responsibility when these galleries are in the vicinity of the railway track. Railway tracks can be considered as the veins of any state/country for different livelihood transportation. Railway contributes a lot to the development of any country for lives and economy. The present study area is located near railway tracks in Tundu of Jogidih Colliery, Jharia Coalfield, Dhanbad (figure 1). According to an old surface mine plan, some mine galleries are expected at a certain distance away from the railway tracks.

Published online: 19 March 2024

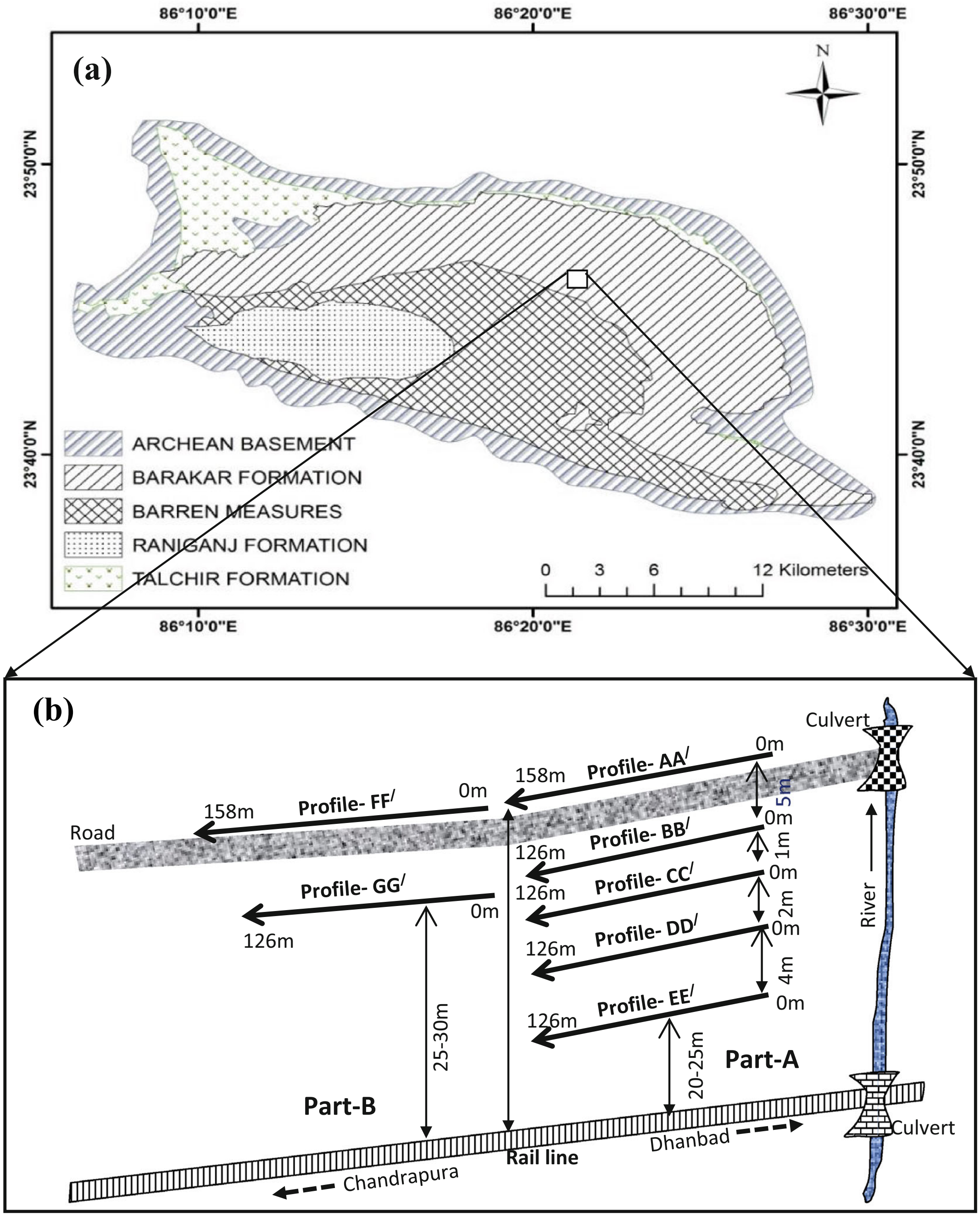

Figure 1. (**a**) Generalized geological map of the Jharia Coalfield (modified after Chandra 1992) and (**b**) schematic layout plan showing tentative locations of ERT profiles.

These galleries are expected to be ∼30 years old and are associated with coal seam-X and seam-XA. These coal seams are expected at a depth of approximately 10–15 m, as indicated in the drilled hole data of the nearby area (figure 2). Subsequently, galleries may have been developed between 10 and 20 m depth through the bord and pillar method. In the bord and pillar method, it is assumed that galleries were excavated for coal production and coal pillars were left for the roof support (Coal Atlas of India 1993). So, we are motivated to perform this study for the safety and security of the railway tracks and nearby areas.

Therefore, parallel to sub-parallel profile lines of ERT were selected for mapping the possible extension of the cavity/gallery/goaf using Flash RES Universal 61 channel instrument, and data were processed using a 2.5D resistivity inversion program. A magnetic survey was performed using a GSM 19T standard portable proton magnetometer

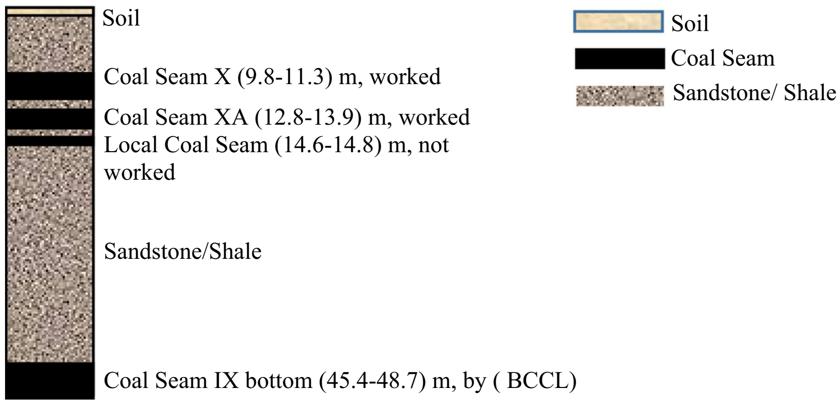

Figure 2. Represents the nearby area bore hole logging data of the Tundu (modified after Das *et al.* 2017).

with GPS, and data were analyzed using Oasis Montaj software. Both techniques are unified to understand better the complex nature of cavities/galleries with unknown depth, dimension, extension, and surrounding area conditions.

Magnetic study with other geophysical methods proved very efficient for cavity/gallery/void detection. Mochales *et al.* (2008) performed a combined study using magnetic, gravity, and ground penetrating radar (GPR) techniques to detect underground cavities in the Zaragoza area of Spain. Near-surface investigation of karstic terrains in Ireland has been achieved successfully using magnetic and resistivity methods by Gibson *et al.* (2004). An integrated geophysical study comprising magnetic, gravity, electromagnetic and resistivity methods was used for the detection of caverns in sandstone by Chamon and Dobereiner (1988). Geophysics offers non-invasive indirect characterization of complex subsurface formations, urging integrated geophysical investigation for higher accuracy (Horo *et al.* 2020, 2021, 2023; Kannaujiya *et al.* 2021).

Different researchers have executed successful studies for detecting cavities/voids using ground-penetrating radar and microgravity (Beres *et al.* 2001; Leucci and De Giorgi 2010). Scholars also accomplished the detection of cavities in the subsurface using microgravity and gravity techniques (Butler 1984; Bishop *et al.* 1997). Self-potential has been used well for cavern studies by Lange (1999). Miller and Steeples (1991) used seismic reflection to detect voids in the coal seams. Miller and Steeples (1994) applied seismic surveys for environmental issues. Scholars like Grandjean and Leparoux (2004) proved the efficacy of the seismic method for the detection of cavities and buried materials. Ge *et al.* (2008) utilized a seam-seismic technique to locate voids in an anthracite mine. Debeglia *et al.* (2006) applied microgravity and MASW for karst investigation in Orléans, France. The MASW method has been evaluated for the assessment of steeply dipping cavities by Xu and Butt (2006). SRT has been used for karst cavities, as conducted by Sheehan *et al.* (2005). Integrated geophysical investigation is quite popular for coal mining studies (Wu *et al.* 2016; Luo *et al.* 2019). In Raniganj and Jharia Coalfields, different geophysical studies have been carried out for sustainable coal mining and mine hazard analysis, mostly using resistivity (Verma and Bhuin 1979; Verma *et al.* 1982; Singh *et al.* 2004; Bharati *et al.* 2015, 2016b, 2019, 2021; Das *et al.* 2017; Srivastava *et al.* 2020; Kumar *et al.* 2021) and magnetic (Vaish and Pal 2015a, b; Pal *et al.* 2016) methods, separately. The present study mainly focuses on mapping the old mine galleries and checking the stable ground formation considering their extension near railway tracks using combined resistivity and magnetic study.

2. Geological setup of the study area

Our study area is a part of Tundu, Jogidih Colliery, Jharia Coalfield, which is west of Dhanbad (figure 1). This study is related to the gallery associated with coal seam-X and seam-XA, which belong to the Barakar Formation. The most prominent coal seams are from the Barakar Formation, which consists of nearly 18 major coal seams. Barakar Formation mainly comprises sandstone of variable grain size, argillaceous sandstone, intercalation of sandstone and shale, carbonaceous shale, jhama, mica-peridotite, and coal seam (Chandra and Chakraborty 1989; Vaish and Pal 2015a, b). Lower Gondwana series includes Talchir, followed by Barakar (lower coal series), then barren measures and uppermost is the Raniganj series (upper coal series), all formations lying above the Archean basement (Fox 1930; Chandra 1992). Jharia Coalfield covers an area of around 450 km^2, a sickle-shaped area with an extension of approximately 19 km from north to south and 38 km from east to west.

3. Methodology

A resistivity survey was performed in the vicinity of the railway tracks to check the stable homogeneous formation and extension of the gallery zone near the railway track. Resistivity data was acquired through 61-channel (64 electrodes) Universal Flash RES instrument with Wenner, Schlumberger, Gradient and Dipole–Dipole arrays. A total of seven profiles were selected for ERT data acquisition (figure 1). The electrode spacing for selected profiles AA′ and FF′ was 2.5 m, covering a length of 158 m. ERT data were collected with 2 m electrode spacing in profiles BB′, CC′, DD′, EE′, and GG′, covering a total distance of 126 m (figure 1b). All the profiles were initiated from the culvert side and terminated at the Chandrapura station side, as indicated in figure 1(b). Wenner array is sensitive to vertical variations and is preferred for finding the horizontal structure (Loke 1999). Schlumberger array is discreetly sensitive to both horizontal and vertical structures (Loke 1999). Dipole–Dipole array is sensitive to horizontal variations, so it is preferred to find a cavity or dyke like structure (Loke 1999). Gradient array with multiple electrode combinations best suits the subsurface structure resolution (Dahlin and Zhou 2004, 2006; Bharti *et al.* 2016b). Resistivity data were filtered with the Flash RES Universal data checking program and processed through a 2.5D resistivity inversion program. After processing all the arrays, the data were combined for a joint inversion to achieve more effective results. It has been established that the inversion of collective datasets acquired by different arrays in the same profile delivers relative benefits for all arrays and yields better results than the individual (De la Vega *et al.* 2003; Stummer *et al.* 2004; Athanasiou *et al.* 2007; Bharti *et al.* 2016a; Das *et al.* 2017). Signal-to-noise ratio and resolution significantly enhanced in the inversion of combined data (Zhou and Greenhalgh 2000; Dahlin and Zhou 2006).

Magnetic data was acquired using a GSM 19T standard portable proton magnetometer with GPS. The sensitivity of the instrument is 0.15 nT/Hz with a resolution of 0.01 and 0.2 nT absolute accuracy. Dense magnetic measurements were performed on and around the expected area for mapping the underground mine gallery. Magnetic data were obtained using a proton precession magnetometer at 2 m data spacing for five profiles spaced 10 m apart, generating high-resolution data. Repeated base readings were taken every two hours, and the magnetic data were corrected for the diurnal variation. Magnetic data utilized in this study were of 99 signal strength.

Further, magnetic data were gridded and processed in the Oasis Montaj software. A total magnetic anomaly (TMA) map was developed by subtracting the IGRF value from the total magnetic intensity (TMI) map. The first-order vertical derivative of TMA data was computed to highlight shallow structures, reducing anomaly complexity and allowing precise imaging of the causative structures (Rao *et al.* 1981; Pal and Majumdar 2015; Vaish and Pal 2015b; Pal *et al.* 2016). The TMA was corrected using the reduced-to-pole (RTP) technique, ensuring the anomaly center on top of its causative sources (Roy and Aina 1986; Ganguli *et al.* 2021a, b, 2022).

4. Results

4.1 *Resistivity study*

In figure 3, 2D ERT cross sections of (a) Wenner, (b) Schlumberger, (c) gradient, (d) dipole–dipole, and (e) joint inversion of all arrays for Profile AA′ are plotted. However, for interpretation purposes, the joint inversion section has been selected, as indicated in figure 10(a). The 2D ERT section shows subsurface resistivity anomaly distributions in Profile AA′ (figure 10a). AH1 indicates a relatively high resistivity (∼300–800 Ωm) feature with a horizontal extension of ∼0–60 m and depth of ∼13–32 m, which may be inferred as high resistive compact ground. AL1 indicates a relatively low resistivity (∼150–200 Ωm) feature with a horizontal extension of ∼60–76 m and depth of ∼15–27 m, which may be inferred as goaf/voids/cavities filled with loose material of relatively higher moisture content. AH2 represents a relatively high resistivity (∼250–350 Ωm) feature with a horizontal extension of ∼70–100 m and depth of ∼8–22 m, which may be

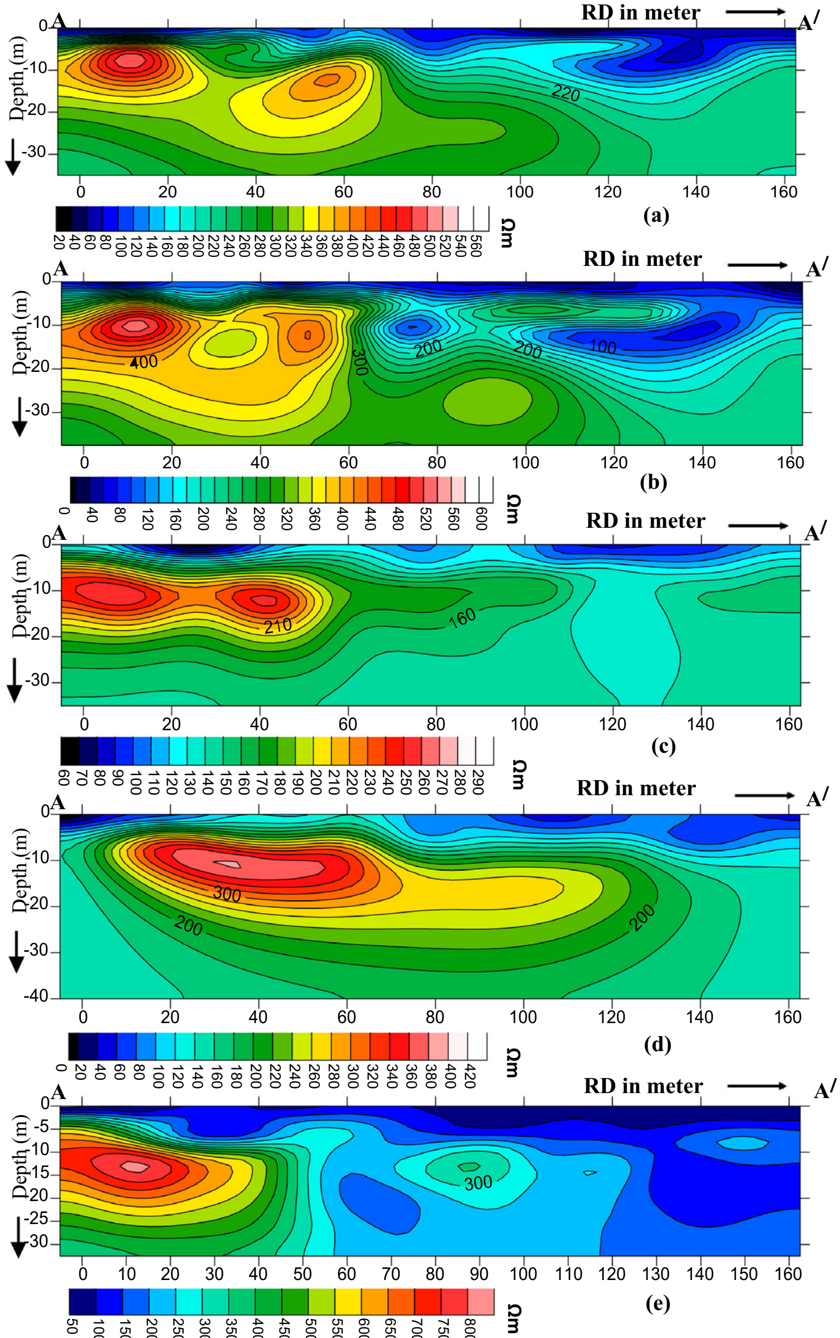

Figure 3. Represents the 2D ERT cross sections of (**a**) Wenner, (**b**) Schlumberger, (**c**) gradient, (**d**) dipole−dipole, and (**e**) joint inversion of all arrays for Profile AA′.

inferred as relatively high resistive compact ground. AL2 represents a relatively low resistivity (∼100–150 Ωm) feature with a horizontal extension of ∼128–160 m and depth of ∼10–25 m, which may be inferred as goaf/voids/cavities filled with loose material of relatively higher moisture content. Details of resistivity features are provided in table 1.

In figure 4, 2D ERT cross sections of (a) Wenner, (b) Schlumberger, (c) gradient, and (d) joint inversion of all arrays for Profile BB′ are plotted. However, the joint inversion section has been selected for interpretation purposes, as indicated in figure 10(b). 2D ERT section shows subsurface resistivity anomaly distributions in Profile BB′ (figure 10b). BH1, a relatively high resistivity feature of ∼280–460 Ωm, has been identified with a horizontal extension of ∼0–33 m and a depth of ∼6–27 m, which may be inferred as high resistive compact ground. BL1, a relatively low resistivity feature of ∼120–160 Ωm, has been observed with a

Table 1. *Describes the approximated resistivity value, extension and depth of the anomalous features of the joint inversion cross-section for different profiles in Part A.*

2D joint inversion ERT section	Name of anomalous feature	Approx. horizontal extension (m)	Approx. depth (m) of anomaly	Approx. resistivity (Ωm)	Possible attributes
Profile AA′ (figure 10a)	AH1	0–55	13–32	300–800	High resistive compact ground
	AL1	60–76	15–27	150–200	Possible goaf/voids/cavities filled with loose material of relatively higher moisture content
	AH2	70–100	8–22	250–350	Relatively high resistive compact ground
	AL2	128–160	10–25	100–150	Possible goaf/voids/cavities filled with loose material of relatively higher moisture content
Profile BB′ (figure 10b)	BH1	0–33	6–27	280–460	High resistive compact ground
	BL1	34–42	8–14	120–160	Possible goaf/voids/cavities filled with loose material of relatively higher moisture content
	BH2	44–108	6–27	200–260	Relatively high resistive compact ground
	BL2	80–84	10–12	140–160	Possible goaf/voids/cavities filled with loose material of relatively higher moisture content
Profile CC′ (figure 10c)	CH1	0–46	7–27	200–460	High resistive compact ground
	CL1	47–58	16–25	160–180	Possible goaf voids/cavities filled with loose material of relatively higher moisture content
	CH2	59–130	5–27	180–320	Relatively high resistive compact ground
	CL2	82–96	9–14	40–80	Possible topsoil cover with loose material of
	CL3	105–117	9–16	40–80	relatively higher moisture content
Profile DD′ (figure 10d)	DH1	0–56	8–27	200–520	High resistive compact ground
	DL1	61–70	7–20	100–180	Possible goaf/voids/cavities filled with loose material of relatively higher moisture content
	DL2	0–130	0–10	100–140	Possible loose material of relatively higher moisture content
	DH2	73–130	16–27	220–300	Relatively high resistive compact ground
Profile EE′ (figure 10e)	EH1	25–130	4–10	150–180	Possible homogeneous compact formation (first layer)
	EH2	0–130	10–27	190	Possible homogeneous compact formation (second layer)

horizontal extension of ∼34–42 m and a depth of ∼8–14 m, which may be inferred as goaf/voids/cavities filled with loose material of relatively higher moisture content. BH2, a relatively high resistivity feature of ∼200–260 Ωm, has been delineated with a horizontal extension of ∼44–108 m and a depth of ∼6–27 m, which may be inferred as relatively high resistive compact ground. BL2, a relatively low resistivity feature of ∼140–160 Ωm, has been delineated with a horizontal extension of ∼80–84 m and a depth of ∼10–12 m, which may be inferred as goaf/voids/cavities filled with loose material of relatively higher moisture content. Details of resistivity features are provided in table 1.

In figure 5, 2D ERT cross sections of (a) Wenner, (b) Schlumberger, (c) gradient, (d) dipole–dipole, and (e) joint inversion of all arrays for Profile CC′ are plotted. However, for interpretation purposes, the joint inversion section has been selected, as indicated in figure 10(c). 2D ERT section indicates subsurface resistivity anomaly distributions in Profile CC′ (figure 10c, table 1). CH1 represents a relatively high resistivity (∼200–460 Ωm) feature

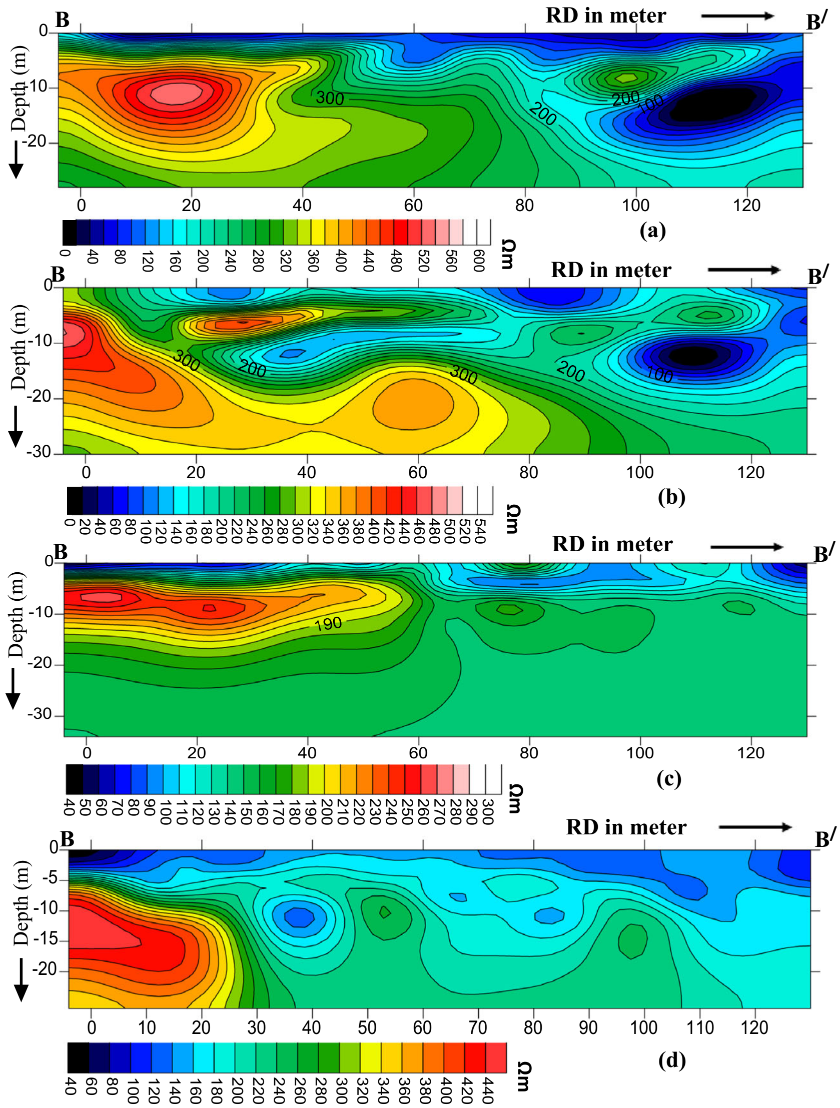

Figure 4. Represents the 2D ERT cross sections of (**a**) Wenner, (**b**) Schlumberger, (**c**) gradient, and (**d**) joint inversion of all arrays for Profile BB′.

with a horizontal extension of ∼0–46 m and a depth of ∼7–27 m, which may be inferred as high resistive compact ground. CL1 represents a relatively low resistivity feature of ∼160–180 Ωm with a horizontal extension of ∼47–58 m and a depth of ∼16–25 m, which may be inferred as goaf/voids/cavities filled with loose material of relatively higher moisture content. CH2 represents a relatively high resistivity feature of ∼180–320 Ωm with a horizontal extension of ∼59–130 m and a depth of ∼5–27 m, which may be inferred as relatively high resistive compact ground. CL2 indicates a relatively low resistivity feature of ∼40–80 Ωm with a horizontal extension of ∼82–96 m and a depth of ∼9–14 m. CL3 shows a relatively low resistivity feature of ∼40–80 Ωm with a horizontal extension of ∼105–117 m, and a depth of ∼9–16 m is observed; both features may be inferred as possible topsoil covered with loose material of relatively higher moisture content.

In figure 6, 2D ERT cross sections of (a) Wenner, (b) Schlumberger, (c) gradient, (d) dipole–dipole, and (e) joint inversion of all arrays for Profile DD′ are plotted. However, for interpretation purposes, the joint inversion section has been selected, as indicated in figure 10(d). The 2D ERT section represents subsurface resistivity anomaly distributions in Profile DD′ (figure 10d, table 1). DH1, a relatively high resistivity (∼200–520 Ωm) feature, has been delineated with a horizontal extension of ∼0–56 m and a depth of ∼8–27 m, which may be inferred as high resistive compact ground. DL1, a relatively low resistivity (∼100–180 Ωm) feature, has been identified with a horizontal extension of

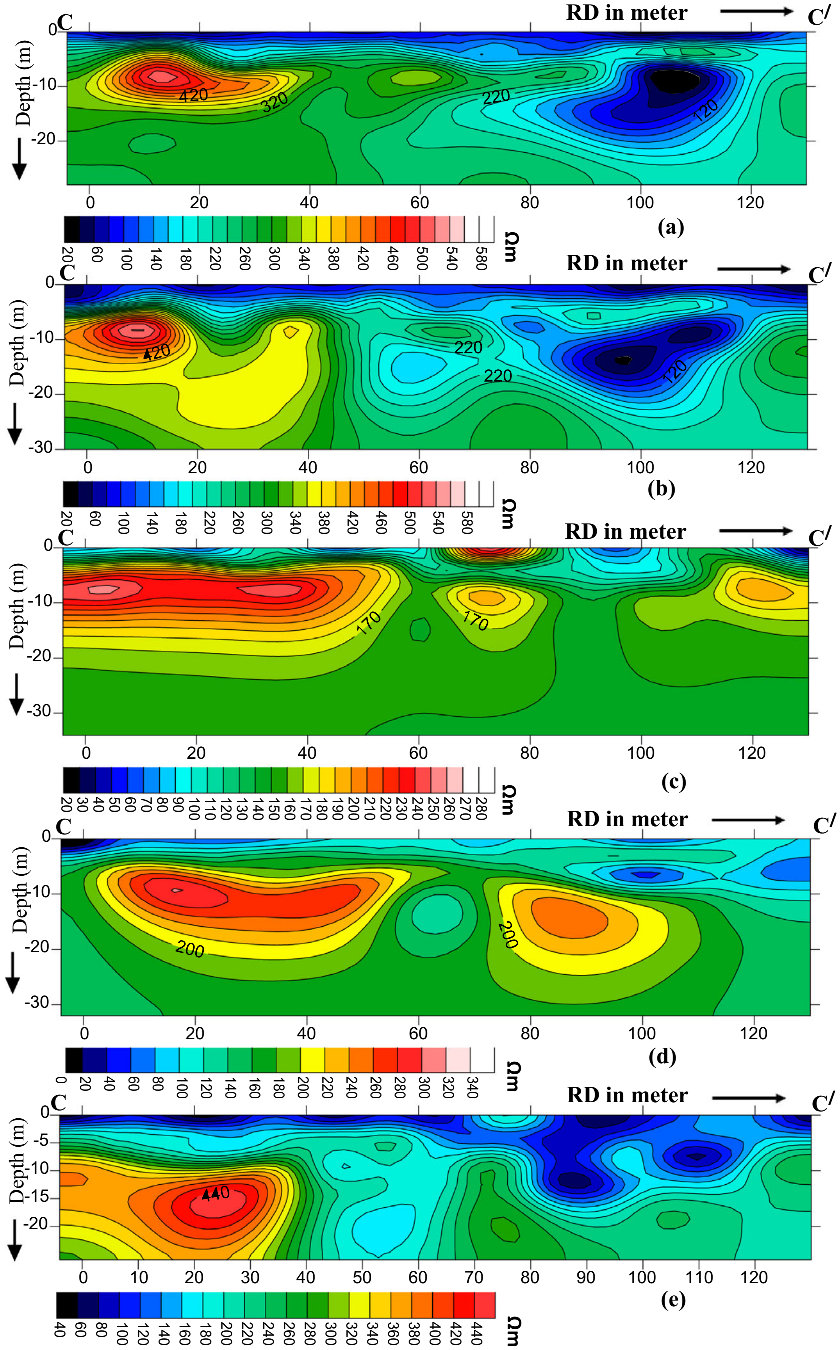

Figure 5. Represents the 2D ERT cross sections of (**a**) Wenner, (**b**) Schlumberger, (**c**) gradient, (**d**) dipole−dipole, and (**e**) joint inversion of all arrays for Profile CC′.

∼61–70 m and a depth of ∼7–20 m, which may be inferred as goaf/voids/cavities filled with loose material of relatively higher moisture content. DH2, a relatively high resistivity (∼220–300 Ωm) feature, has been delineated with a horizontal extension of ∼73–130 m and a depth of ∼16–27 m, which may be inferred as relatively high resistive compact ground. DL2, a relatively low resistivity (∼100–140 Ωm) feature, has been delineated with a horizontal extension of ∼0–130 m and a depth of ∼0–10 m, which may be inferred as possible loose material of relatively higher moisture content.

In figure 7, 2D ERT cross sections of (a) Wenner, (b) Schlumberger, (c) gradient, (d) dipole–dipole, and (e) joint inversion of all arrays for Profile EE′ are plotted. However, for interpretation purposes, the joint inversion section has been selected, as indicated in figure 10(e). 2D ERT section shows subsurface resistivity anomaly distributions in Profile EE′ (figure 10e, table 1). EH1, a relatively

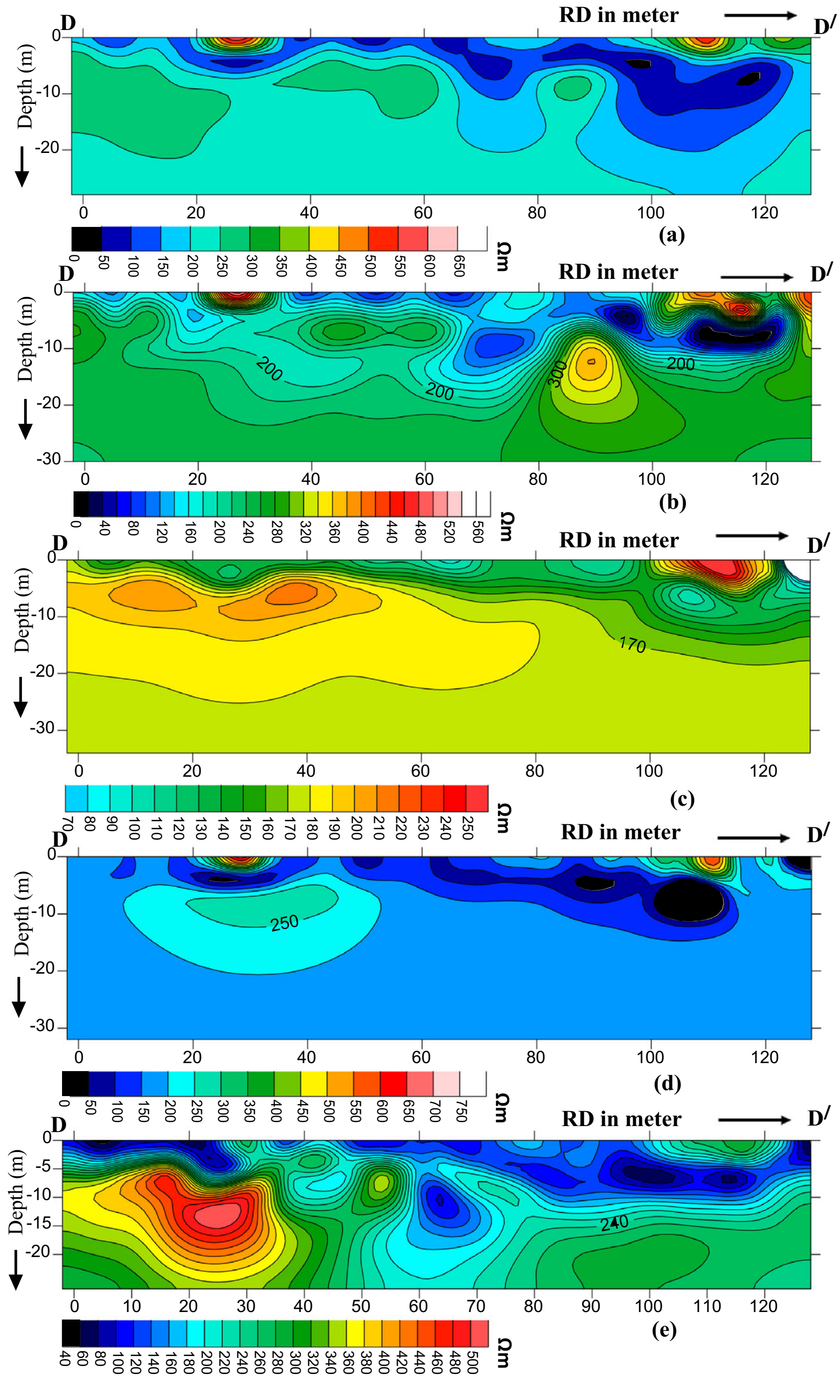

Figure 6. Represents the 2D ERT cross sections of (**a**) Wenner, (**b**) Schlumberger, (**c**) gradient, (**d**) dipole−dipole, and (**e**) joint inversion of all arrays for Profile DD′.

high resistivity feature of ∼150–180 Ωm, has been observed with a horizontal extension of ∼25–130 m and a depth of ∼4–10 m, which may be inferred as a possible homogeneous compact formation (first layer). EH2 represents a relatively higher resistivity feature of ∼190 Ωm with a horizontal extension of ∼0–130 m and a depth of ∼10–27 m, which may be inferred as a possible homogeneous compact formation (second layer).

In figure 8, 2D ERT cross sections of (a) gradient, (b) dipole–dipole, and (c) joint inversion of both arrays for Profile FF′ are plotted. However, for interpretation purposes, the joint inversion section has been selected, as indicated in figure 10(f). 2D ERT section indicates subsurface resistivity anomaly distributions in Profile FF′ (figure 10f, table 2). FH1, a relatively high resistivity (∼100–120 Ωm) feature, has been delineated

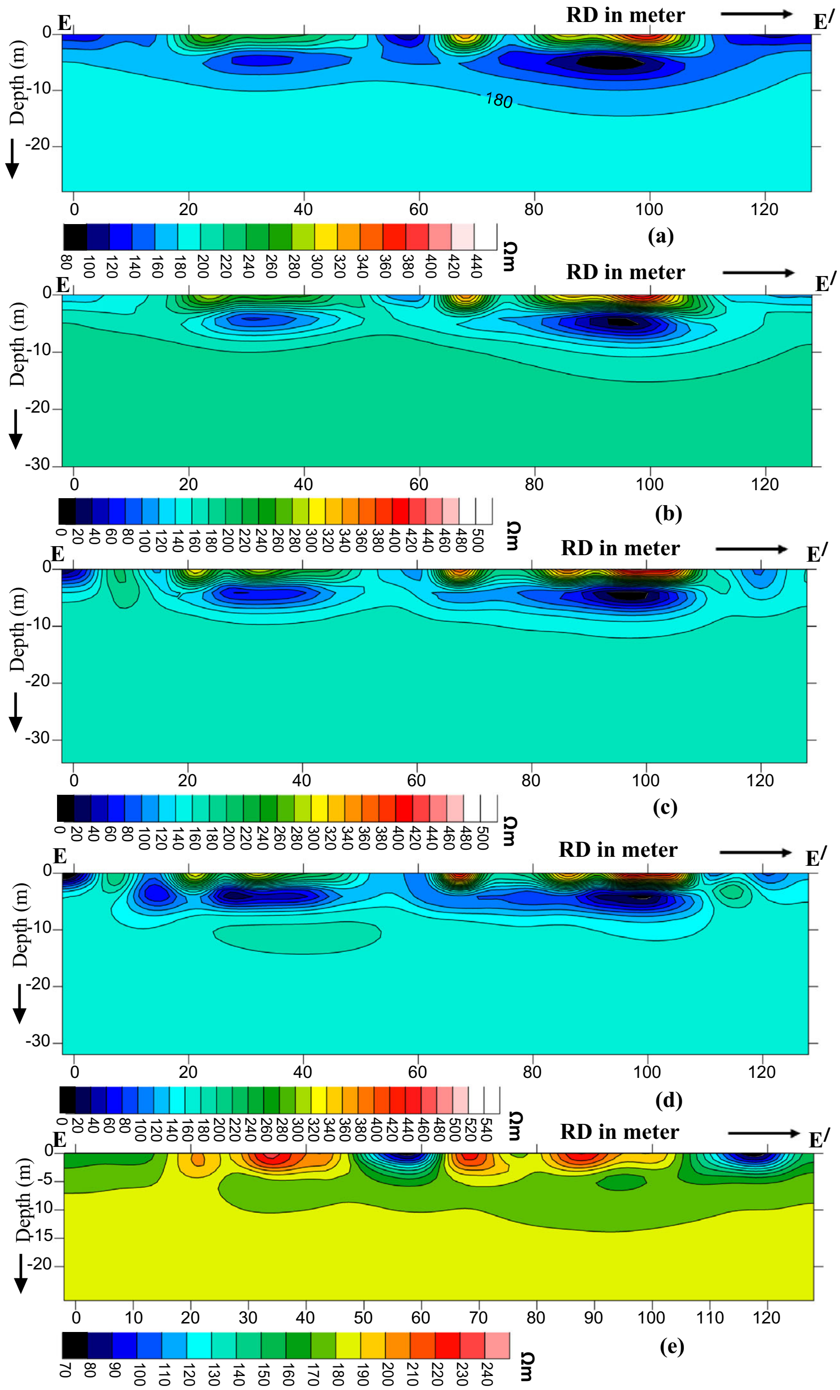

Figure 7. Represents the 2D ERT cross sections of (**a**) Wenner, (**b**) Schlumberger, (**c**) gradient, (**d**) dipole−dipole, and (**e**) joint inversion of all arrays for Profile EE′.

with a horizontal extension of ∼0–160 m and a depth of ∼0–13 m, which may be inferred as a possible homogeneous compact formation (first layer). FL1, a relatively low resistivity (∼70–85 Ωm) feature, has been identified with a horizontal extension of ∼0–160 m and a depth of ∼15–32 m, which may be inferred as possible goaf/voids/cavities filled with loose material of relatively higher moisture content (second layer).

In figure 9, 2D ERT cross sections of (a) Wenner, (b) Schlumberger, (c) gradient, (d) dipole–dipole, and (e) joint inversion of all arrays for Profile GG′ are plotted. However, for interpretation purposes, the joint inversion section has been selected, as indicated in figure 10(g). The 2D ERT section represents subsurface resistivity anomaly distributions in Profile GG′ (figure 10g, table 2). GL1 indicates a relatively low resistivity feature of ∼40–120 Ωm

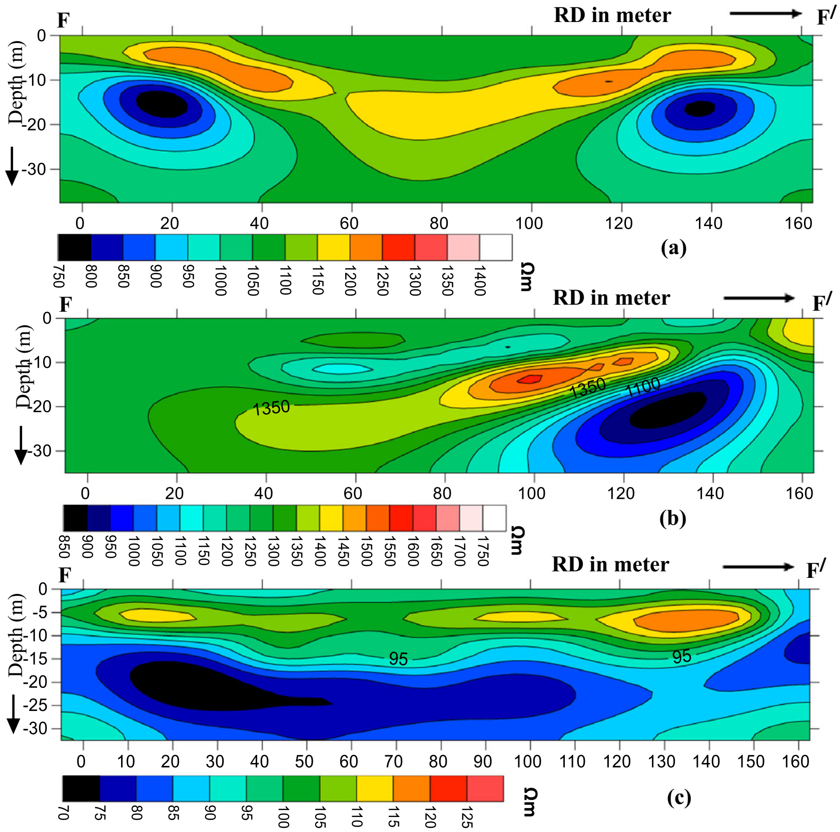

Figure 8. Represents the 2D ERT cross sections of (**a**) gradient, (**b**) dipole–dipole, and (**c**) joint inversion of all arrays for Profile FF′.

Table 2. *Describes the approximated resistivity value, extension, and depth of the anomalous features of the joint inversion cross-section for different profiles in Part B.*

2D joint inversion ERT section	Name of anomalous feature	Approx. horizontal extension of anomaly (RD in m)	Approx. depth (m) of anomaly	Approx. resistivity (Ωm)	Remarks
Profile FF′ (figure 10f)	FH1	0–160	0–13	100–120	Possible homogeneous compact formation (first layer)
	FL1	0–160	15–32	70–85	Possible goaf/voids/cavities filled with loose material of relatively higher moisture content
Profile GG′ (figure 10g)	GL1	0–160	0–6	40–120	Topsoil cover with loose material of relatively higher moisture content
	GH1	0–160	6–27	160–320	Possible homogeneous compact formation

with a horizontal extension of ∼0–160 m and a depth of ∼0–6 m, which may be inferred as topsoil covered with loose material of relatively higher moisture content (first layer). GH1 indicates a relatively high resistivity feature of ∼160–320 Ωm with a horizontal extension of ∼0–160 m and a depth of ∼6–27 m, which may be inferred as a possible homogeneous compact formation (second layer).

4.2 *Magnetic study*

The TMA map of the present study area is shown in figure 11. A low magnetic anomaly over the expected area has been observed, possibly indicating gallery locations marked by the black dashed line. Magnetic anomaly varies from –350.8 to –176.1 nT near the possible gallery/void.

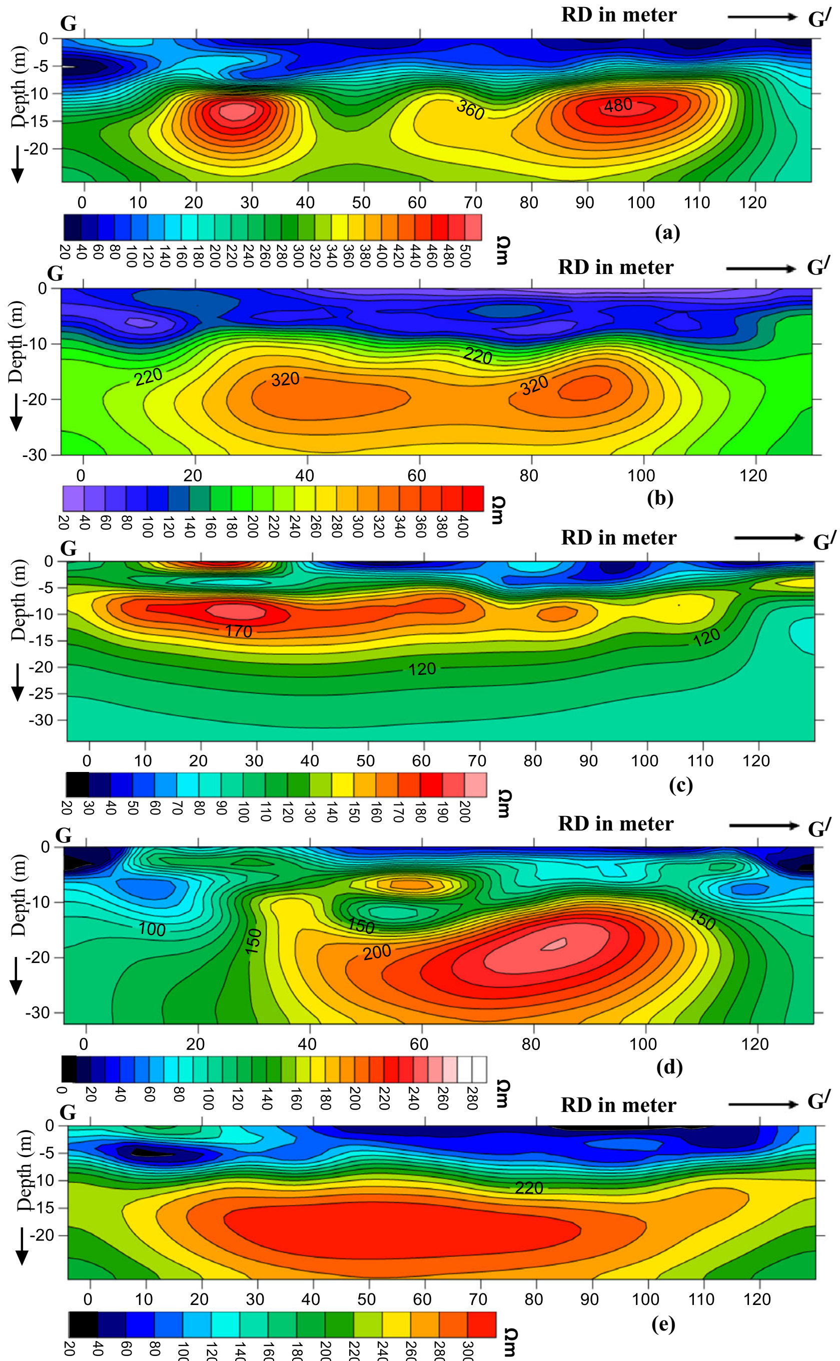

Figure 9. Represents the 2D ERT cross sections of (**a**) Wenner, (**b**) Schlumberger, (**c**) gradient, (**d**) dipole–dipole, and (**e**) joint inversion of all arrays for Profile GG′.

The RTP of the TMA map is shown in figure 12. A broad low magnetic anomaly zone (–517.6 to –200 nT) has been identified over the expected area of the possible old gallery, marked by a black dashed polygon.

The first vertical derivative (FVD) of the TMA map is shown in figure 13, which clearly delineates 11 low magnetic anomalies (–24.5 to –10.9 nT/m) over the expected area of possible gallery/void shown by the dashed circle with 1–11 numbering for each possible gallery. The low anomaly may be due to natural wear and tear in the galleried zone over time. This phenomenon of low anomaly may be due to the loose material or absence of material.

5. Discussions

A comprehensive analysis has been carried out using ERT and magnetic methods. For simplification, the entire area has been studied using ERT

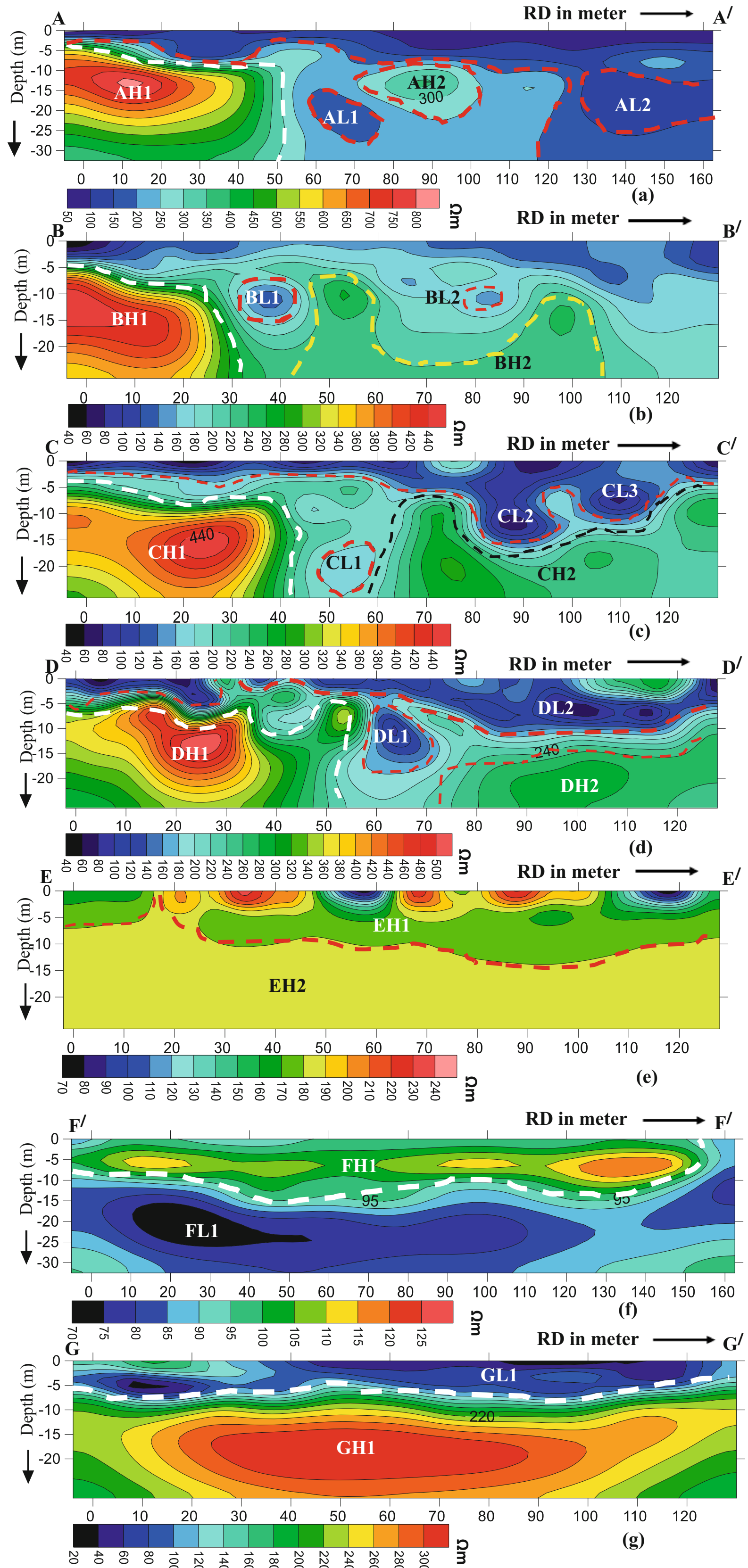

Figure 10. Represents joint inversion of profiles AA′, BB′, CC′, DD′, EE′, FF′, and GG′ for figures (**a**), (**b**), (**c**), (**d**), (**e**), (**f**), and (**g**), respectively.

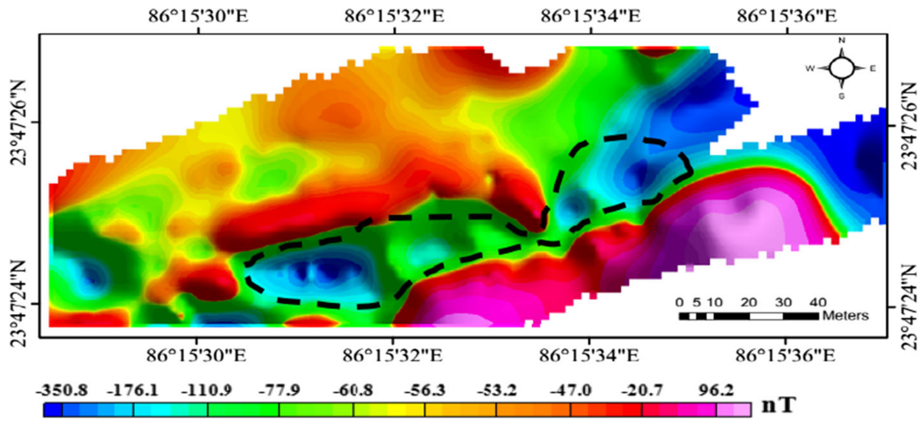

Figure 11. Total magnetic anomaly map of the study area. A black dashed polygon shows a possible broad zone of underground galleries.

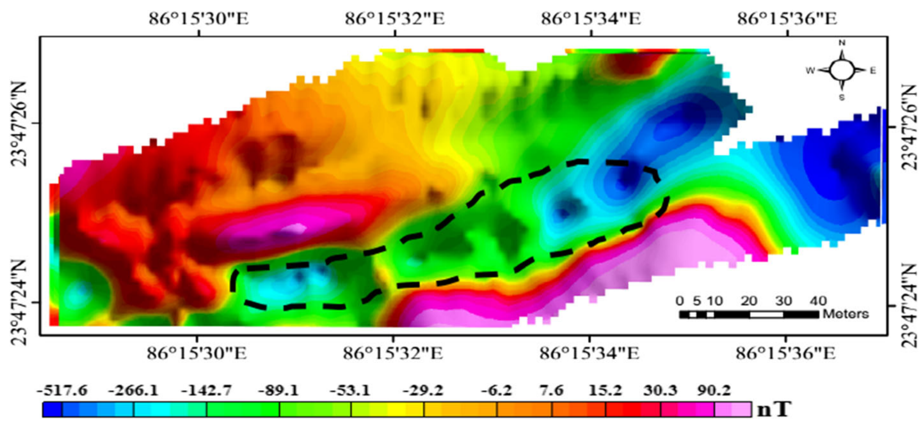

Figure 12. Reduced to pole (RTP) of total magnetic anomaly (TMA) map. A black dashed polygon shows a possible broad zone of underground galleries.

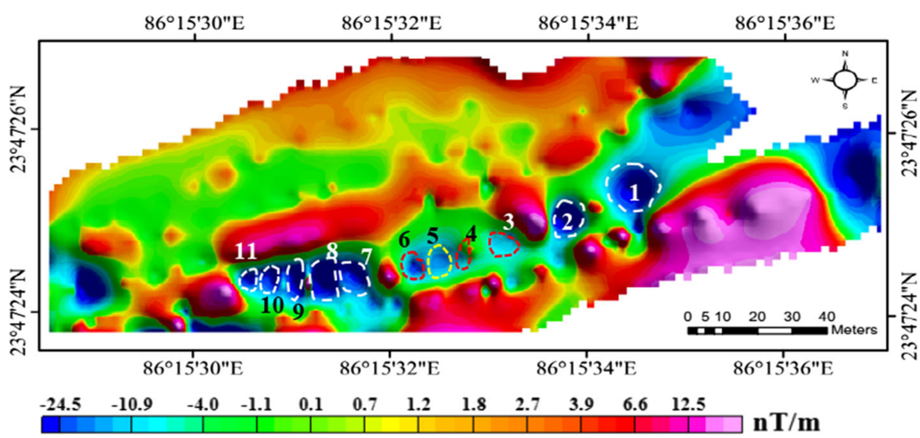

Figure 13. First vertical derivative of total magnetic anomaly map.

considering two parts, Part A and Part B. 2D ERT sections were generated along parallel and sub-parallel profile lines on Part A and Part B to detect cavity/gallery/goaf with their extension. Our concern for the study is also to check the stable subsurface formation of the area within ∼25 m from the railway tracks, considering homogeneous underneath formation. The details of distinct resistive anomalous features delineated in Part A and Part B have been summarized in tables 1 and 2, respectively. Based on the variation of relative resistivity anomaly, different zones have

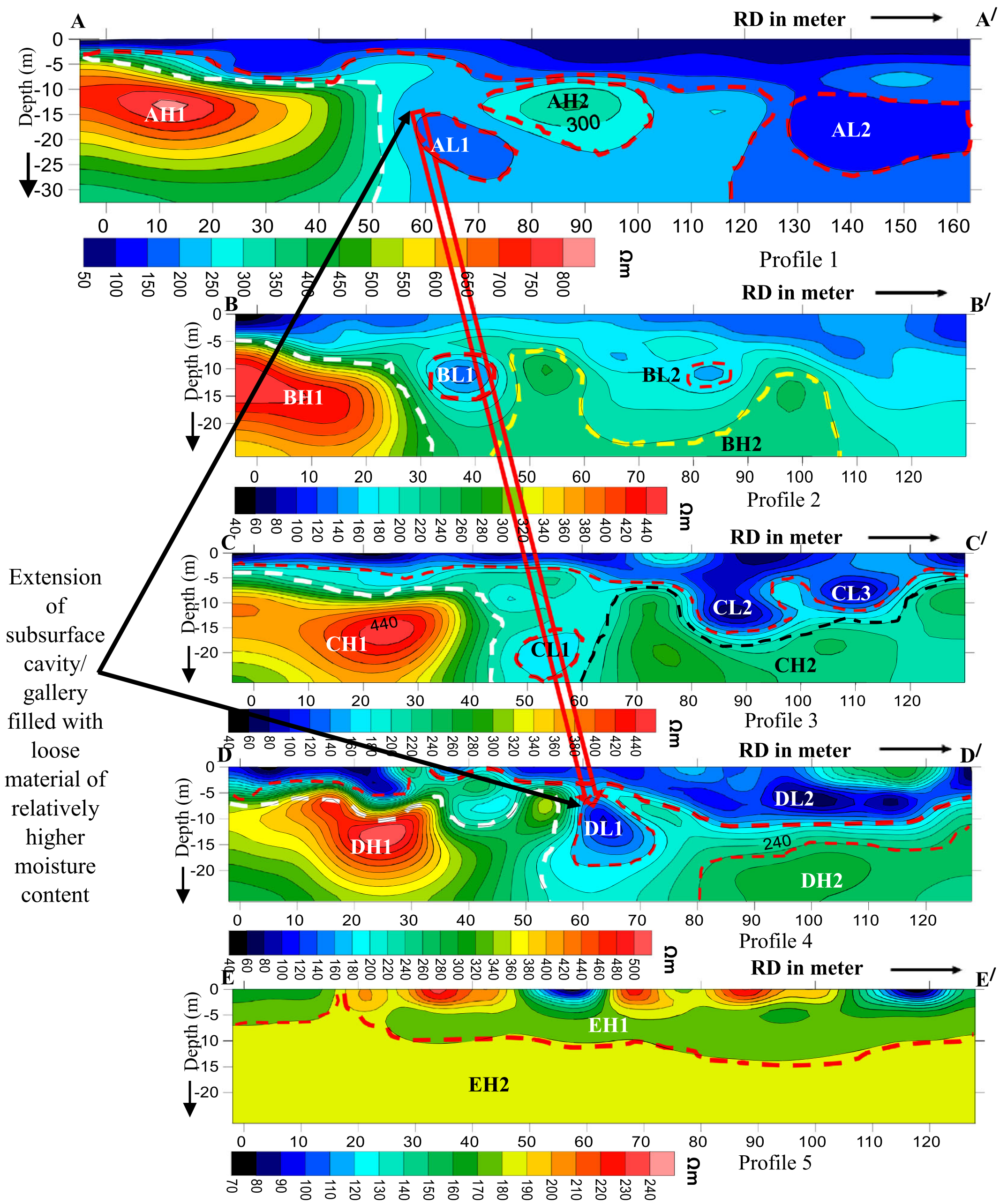

Figure 14. An integrated model of 2D ERT sections of subsurface resistivity (Ωm) variation for joint inversion profiles AA′, BB′, CC′, DD′, and EE′ (Part A) showing the tentative extension of subsurface cavity/gallery/goaf filled with loose material of relatively higher moisture content.

been identified, including (i) a possible solid high-resistive compact ground, (ii) a possible cavity/gallery/goaf filled with water or loose material with relatively higher moisture content, and (iii) a possible topsoil covered with higher moisture content or saturated by water.

A schematic geoelectrical model of Part A generated using 2D ERT sections of subsurface resistivity (Ωm) variation for profiles AA′, BB′, CC′, DD′, and EE′ indicating the tentative extension of subsurface cavity/gallery/goaf filled with water or loose material of relatively higher moisture content, is presented in figure 14. A schematic geoelectrical model covering parts of Part A and Part B is shown in figure 15. 2D ERT sections of subsurface resistivity (Ωm) variation delineates the tentative location of solid homogeneous formation. Imprints of the possible galleries have been identified at a certain distance away from the railway tracks using magnetic, which corresponds well with

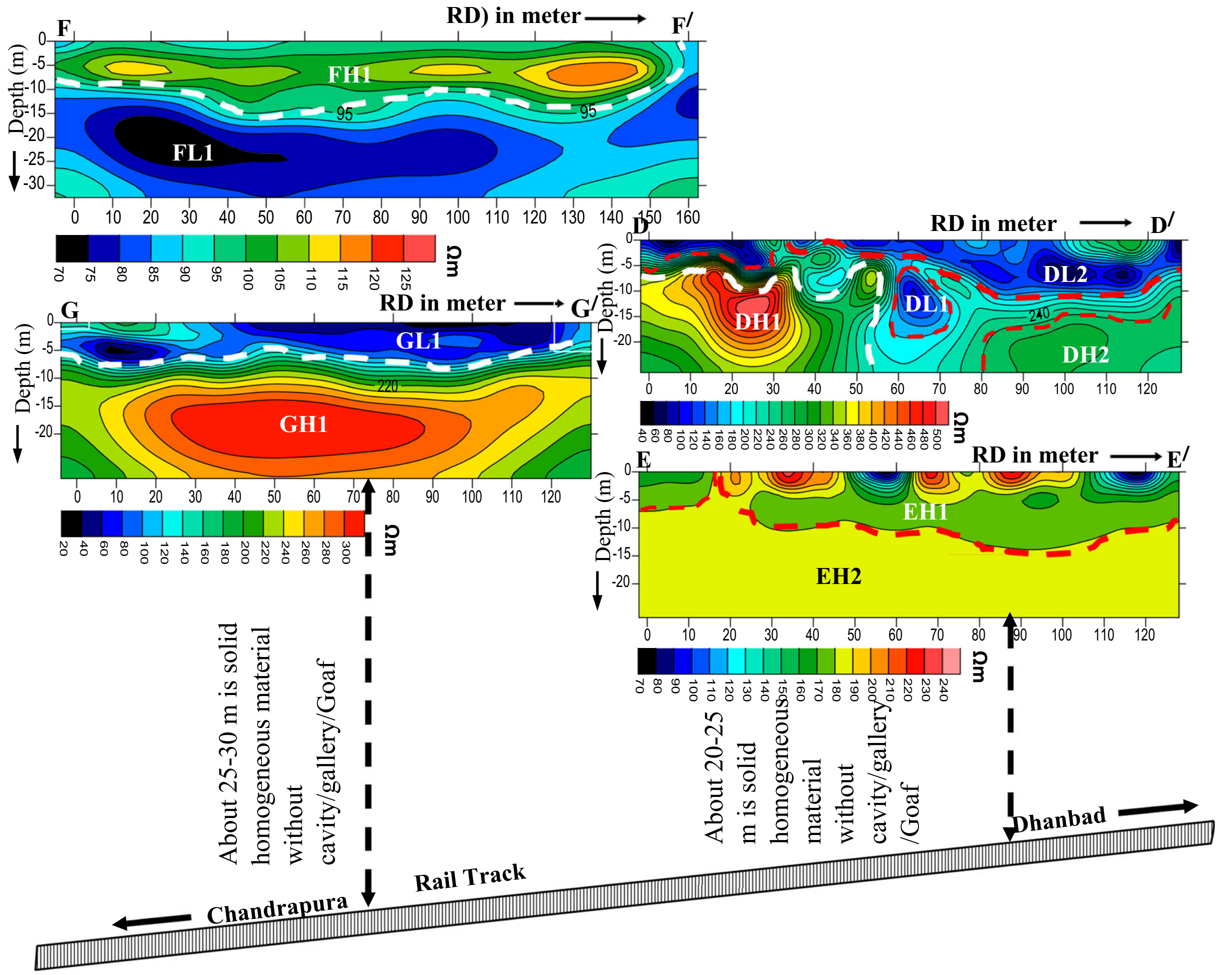

Figure 15. An inferred model of 2D ERT sections of subsurface resistivity (Ωm) variation showing the tentative location of solid homogeneous materials.

the schematic old mine plan of BCCL, as shown in figure 16. A relatively high magnetic anomaly zone was observed beside railway tracks, which may indicate the absence of galleries/voids/goaves, and the presence of homogeneous compact ground. No recent drilling was performed for the report verifications; however, the approximate depth range identified in the present study corroborates well with the old drilled hole data available around the study area, indicating coal seam-X and seam-XA with depth ranging from about 10 to 15 m.

Using the ERT study, it has been inferred that ground within 20–25 m from the railway line in Part A is a possible homogeneous compact formation without any cavity/gallery/goaf. Meanwhile, the ground within 25–30 m from the railway line in Part B has also been inferred to be a possible homogeneous compact formation without any cavity/gallery/goaf. So, unifying ERT and magnetic studies, it is inferred that ground within the area of ∼20 m from the railway tracks is stable due to homogeneous compact ground as there is no gallery.

6. Conclusions

- The comprehensive ERT study suggests different subsurface zones, such as (i) relatively high resistive feature possibly indicates homogeneous/solid compact ground, (ii) relatively low resistive feature possibly indicates cavity/gallery/goaf filled with water-saturated formation/loose formation of relatively higher moisture content, and (iii) moderately low resistive feature indicates possible topsoil covered with higher moisture content/saturated by water; considering relative resistivity distribution.
- A broad low magnetic anomaly zone has been identified that corresponds well with the broad low resistivity anomaly pattern associated with possible galleries of the study area. The first vertical

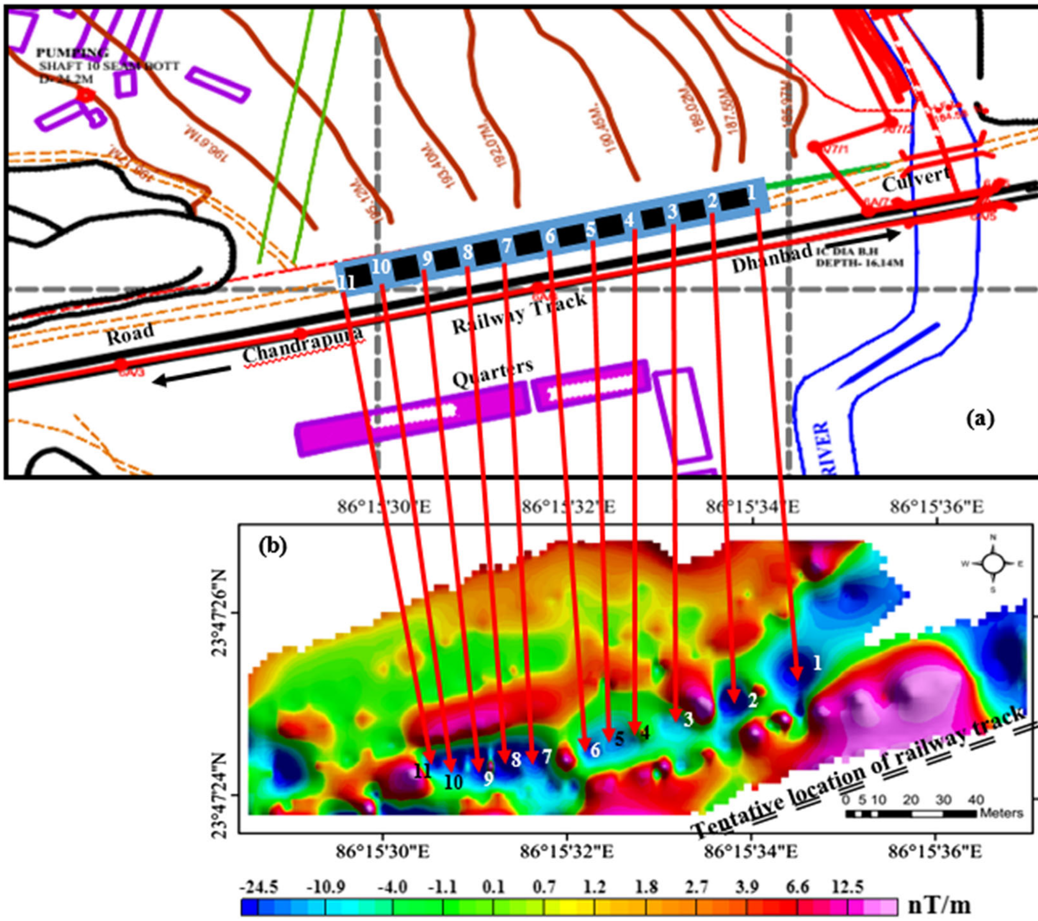

Figure 16. Correlation of the galleries from (**a**) schematic tentative galleries surfaces mine plan of the site in Tundu Khaas, Jogidih Colliery, source (BCCL) to (**b**) first vertical derivative map.

derivative of the TMA map delineates 11 low magnetic anomalies, indicating possible location and extension of galleries/voids, which corresponds well with the schematic old mine plan of BCCL.

- ERT sections failed to delineate prominent imprints of the 11 galleries separately as identified in the magnetic field, as the ERT lines may not align along the suspected area observed in the first vertical derivative of the TMA. Moreover, the imprints of the galleries may be partially averaged out/smoothened, leading to an extended zone of low resistivity in the ERT section AA′ and FF′.
- The ground within 20–25 m from the railway line in Part A and the ground within 25–30 m from the railway line in Part B are characterized by relatively higher and homogeneous resistivity with higher magnetic anomaly distribution, possibly indicating homogeneous compact formation without any cavity/gallery/goaf.
- So, unifying ERT and magnetic studies, it is inferred that ground within the area of ∼20 m from the railway tracks is stable due to homogeneous compact ground as there is no gallery.

Acknowledgements

The authors are grateful to the Editorial Team, the Journal of Earth System Science and the distinguished anonymous reviewers for their quick, comprehensive review and thoughtful suggestions for improving the manuscript. The authors are grateful to the Director, IIT (ISM) Dhanbad and HOD, Department of Applied Geophysics, for allowing them to carry out this study and providing all the technical help needed. The authors are thankful to ISRO, Department of Space, Government of India, for funding project ISRO/RES/630/2016-17; Ministry of Coal, Government of India, for funding project CMPDI/B&PRO/MT-173; and Department of Science and Technology, Government of India, for funding project nos. SB/S4/ES-640/2012, FST/ES-I/2017/12, and DST/TDT/SHRI-16/2021 (C&G).

Author statement

Saurabh Srivastava: Conceptualization; methodology, writing – original draft preparation, data preparation, interpretation. Rajwardhan Kumar: Data preparation, interpretation. Sanjit Kumar Pal: Conceptualization, methodology, formal analysis and investigation, writing – review and editing, interpretation, supervision. R M Bhattacharjee: Formal analysis, interpretation and supervision.

References

Athanasiou E N, Tsourlos P I, Papazachos C B and Tsokas G N 2007 Combined weighted inversion of electrical resistivity data arising from different array types; *J. Appl. Geophys.* **62** 124–140.

Beres M, Luetscher M and Olivier R 2001 Integration of ground-penetrating radar and microgravimetric methods to map shallow caves; *J. Appl. Geophys.* **46** 249–262.

Bharti A K, Pal S K, Priyam P, Narayan S, Pathak V K and Sahoo S D 2015 *Detection of illegal mining over Raniganj coalfield using electrical resistivity tomography*; Engineering Geology in New Millennium, New Delhi.

Bharti A K, Pal S K, Priyam P, Kumar S, Shalivahan S and Yadav P K 2016a Subsurface cavity detection over Patherdih Colliery, Jharia Coalfield, India using electrical resistivity tomography; *Environ. Earth. Sci.* **75** 1–17.

Bharti A K, Pal S K, Priyam P, Pathak V K, Kumar R and Ranjan S K 2016b Detection of illegal mine voids using electrical resistivity tomography: The case-study of Raniganj Coalfield (India); *Eng. Geol.* **213** 120–132.

Bharti A K, Pal S K, Saurabh, Kumar S, Mondal S, Singh K K K and Singh P K 2019 Detection of old mine workings over a part of Jharia Coalfield, India using electrical resistivity tomography; *J. Geol. Soc. India* **94** 290–296.

Bharti A K, Prakash A, Verma A and Singh K K K 2021 Assessment of hydrological condition in strata associated with old mine working during and post-monsoon using electrical resistivity tomography: A case study; *Bull. Eng. Geol. Environ.* **80** 5159–5166.

Bishop S P, Emsley S J and Ferguson N S 1997 The detection of cavities using the microgravity technique: Case histories from mining and karstic environments; *Geol. Soc. Lond. Eng. Geol. Spec.* **12** 153–166, https://doi.org/10.1144/GSL.ENG.1997.012.01.13.

Butler D K 1984 Microgravity and gravity gradient techniques for detection of subsurface cavities; *Geophysics* **49** 1084–1096.

Chamon N and Dobereiner L 1988 An example of the use of geophysical methods for the investigation of a cavern in sandstones; *Bull. Eng. Geol. Environ.* **38** 37–43.

Chandra D 1992 *Jharia Coalfields*; Geological Society of India, Bangalore, 149p.

Chandra D and Chakraborty N C 1989 Coalification trends in Indian coals; *Int. J. Coal Geol.* **13** 413–435.

Coal Atlas of India 1993 Central Mine Planning Design Institute Publications, Ranchi, pp. 1–139.

Dahlin T and Zhou B 2004 A numerical comparison of 2D resistivity imaging with 10 electrode arrays; *Geophys. Prospect.* **52** 379–398.

Dahlin T and Zhou B 2006 Multiple-gradient array measurements for multichannel 2D resistivity imaging; *Near Surf. Geophys.* **4** 113–123.

Das P, Pal S K, Mohanty P R, Priyam P, Bharti A K and Kumar R 2017 Abandoned mine galleries detection using electrical resistivity tomography method over Jharia Coalfield, India; *J. Geol. Soc. India* **90** 169–174.

De la Vega M, Osella A and Lascano E 2003 Joint inversion of Wenner and dipole–dipole data to study a gasoline-contaminated soil; *J. Appl. Geophys.* **54** 97–109.

Debeglia N, Bitri A and Thierry P 2006 Karst investigations using microgravity and MASW: Application to Orléans, France; *Near Surf. Geophys.* **2** 215–225.

Fox C S 1930 The Jharia Coalfield; *Geol. Surv. India Memoir* **56** 255.

Ganguli S S, Pal S K, Singh S L, Rama Rao J V and Balakrishna B 2021a Insights into crustal architecture and tectonics across Palghat Cauvery Shear Zone, India from combined analysis of gravity and magnetic data; *Geol. J.* **56** 2041–2059.

Ganguli S S, Pal S K, Sundaralingam K and Kumar P 2021b Insights into the crustal architecture from the analysis of gravity and magnetic data across Salem–Attur Shear Zone (SASZ), Southern Granulite Terrane (SGT), India: An evidence of accretional tectonics; *Episodes* **44** 419–442, https://doi.org/10.18814/epiiugs/2020/020095.

Ganguli S S, Mondal S, Pal S K, Lakshamana M and Mahender S 2022 Combined analysis of remote sensing, gravity and magnetic data across Moyar Bhavani Shear Zone, Southern Granulite Terrane (SGT), India: Appraisals for crustal architecture and tectonics; *Geocarto Int.* **37** 13,973–14,004, https://doi.org/10.1080/10106049.2022.2086627.

Ge M, Wang H, Hardy H R and Ramani R 2008 Void detection at an anthracite mine using an in-seam seismic method; *Int. J. Coal Geol.* **73** 201–212.

Gibson P J, Lyle P and George D M 2004 Application of resistivity and magnetometry geophysical techniques for near-surface investigations in karstic terranes in Ireland; *J. Cave Karst Stud.* **66** 35–38.

Grandjean G and Leparoux D 2004 The potential of seismic methods for detecting cavities and buried objects: Experimentation at a test site; *J. Appl. Geophys.* **56** 93–106.

Horo D, Pal S K, Singh S and Saurabh 2020 Combined self-potential, electrical resistivity tomography and induced polarisation for mapping of gold prospective zones over a part of Babaikundi–Birgaon Axis, North Singhbhum Mobile Belt, India; *Explor. Geophys.* **51** 507–522.

Horo D, Pal S K and Singh S 2021 Mapping of gold mineralization in Ichadih, North Sighbhum Mobile Belt, India using Electrical Resistivity Tomography and self-potential methods; *Min. Metall. Explor.* **38** 397–411.

Horo D, Pal S K, Singh S and Biswas A 2023 New insights into the gold mineralization in the Babaikundi–Birgaon Axis, North Singhbhum Mobile Belt, Eastern Indian

Shield using magnetic, very low-frequency electromagnetic (VLF-EM), and self-potential data; *Minerals* **13** 1289.

Kannaujiya S, Philip G, Champati Ray P K and Pal S K 2021 Integrated geophysical techniques for subsurface imaging of active deformation across the Himalayan Frontal Thrust in Singhauli, Kala Amb, India; *Quat. Int.* **575–576** 72–84.

Kumar R, Pal S K and Gupta P K 2021 Water seepage mapping in an underground coal-mine barrier using self-potential and electrical resistivity tomography; *Mine Water Environ.* **40** 622–638.

Lange A L 1999 Geophysical studies at Kartchner Caverns State Park, Arizona; *J. Cave Karst Stud.* **61** 68–72.

Leucci G and De Giorgi L 2010 Microgravity and ground penetrating radar geophysical methods to map the shallow karstic cavities network in a coastal area (Marina Di Capilungo, Lecce, Italy); *Explor. Geophys.* **41** 178–188.

Loke M H 1999 Electrical imaging surveys for environmental and engineering studies: A practical guide to 2-D and 3-D surveys, 67p.

Luo X, Gong S, Huo Z, Li H and Ding X 2019 Application of comprehensive geophysical prospecting method in the exploration of coal mined-out areas; *Adv. Civ. Eng.* **2019** 1–17.

Miller R D and Steeples D W 1991 Detecting voids in a 0.6 m coal seam, 7 m deep, using seismic reflection; *Geoexploration* **28** 109–119.

Miller R D and Steeples D W 1994 Applications of shallow high-resolution seismic reflection to various environmental problems; *J. Appl. Geophys.* **31** 65–72.

Mochales T, Casas A M, Pueyo E L, Pueyo O, Román M T, Pocoví A, Soriano M A and Ansón D 2008 Detection of underground cavities by combining gravity, magnetic and ground penetrating radar survey: A case study from the Zaragoza area, NE Spain; *Environ. Geol.* **53** 1067–1077.

Pal S K and Majumdar T J 2015 Geological appraisal over the Singhbhum–Orissa Craton, India using GOCE, EIGEN6-C2 and in-situ gravity data; *Int. J. Appl. Earth Obs. Geoinf.* **35** 96–119.

Pal S K, Vaish J, Kumar S and Bharti A K 2016 Coalfire mapping of East Basuria Colliery, Jharia Coalfield using vertical derivative technique of magnetic data; *J. Earth Syst. Sci.* **125** 165–178.

Rao D A, Babu H V and Narayan P V 1981 Interpretation of magnetic anomalies due to dikes: The complex gradient method; *Geophysics* **46** 1572–1578.

Roy A and Aina A O 1986 Some new magnetic transformations; *Geophys. Prospect.* **34** 1219–1232.

Sheehan J R, Doll W E, Watson D B and Mandell W A 2005 Application of seismic refraction tomography to karst cavities; US Geological Survey karst interest group proceedings, Rapid City, South Dakota, pp. 29–38.

Singh K K K, Singh K B, Lokhande R D and Prakash A 2004 Multi-electrode resistivity imaging technique for the study of coal seam; *J. Sci. Ind. Res.* **63** 927–930.

Srivastava S, Pal S K and Kumar R 2020 A time-lapse study using self-potential and electrical resistivity tomography methods for mapping of old mine working across railway-tracks in a part of Raniganj Coalfield, India; *Environ. Earth Sci.* **79** 1–19.

Stummer P, Maurer H and Green A 2004 Experimental design: Electrical resistivity data sets that provide optimum subsurface information; *Geophysics* **69** 120–139.

Vaish J and Pal S K 2015a Subsurface coal fire mapping of East Basuria Colliery, Jharkhand; *J. Geol. Soc. India* **86** 438–444.

Vaish J and Pal S K 2015b Geological mapping of Jharia coalfield, India using GRACE EGM 2008 gravity data: A vertical derivative approach; *Geocarto Int.* **30** 388–401.

Verma R K and Bhuin N C 1979 Use of electrical resistivity methods for study of coal seams in parts of the Jharia Coalfields, India; *Geoexploration* **17** 163–176.

Verma R K, Bandopadhyay T K and Bhuin N C 1982 Use of electrical resistivity methods for the study of coal seams in parts of the Raniganj Coalfields (India); *Geophys. Prospect.* **30** 115–126.

Wu G, Yang G and Tan H 2016 Mapping coalmine goaf using transient electromagnetic method and high density resistivity method in Ordos City, China; *Geod. Geodyn.* **7** 340–347.

Xu C and Butt S D 2006 Evaluation of MASW techniques to image steeply dipping cavities in laterally in homogeneous terrain; *J. Appl. Geophys.* **59** 106–116.

Zhou B and Greenhalgh S A 2000 Crosshole resistivity tomography using different electrode configurations; *Geophys. Prospect.* **48** 887–912.

Corresponding editor: Arkoprovo Biswas